Combination of UAV and terrestrial photogrammetry to assess rapid glacier evolution and map glacier hazards

Fugazza, Davide[1]; Scaioni, Marco[2]; Corti, Manuel[2]; D'Agata, Carlo[3]; Azzoni, Roberto Sergio[3]; Cernuschi, Massimo[4]; Smiraglia, Claudio[1]; Diolaiuti, Guglielmina Adele[3]

[1]Department of Earth Sciences 'A.Desio', Università degli studi di Milano, 20133 Milano Italy

[2]Department of Architecture, Built Environment and Construction Engineering, Politecnico di Milano, 20133 Milano Italy

[3]Department of Environmental science and policy (DESP), Università degli studi di Milano, 20133 Milano Italy

[4]Agricola 2000 S.C.P.A., 20067 Tribiano (MI) Italy

Correspondence to: Marco Scaioni (marco.scaioni@polimi.it)

Abstract

Tourists and hikers visiting glaciers all year round face hazards such as sudden terminus collapses, typical of such a dynamically evolving environment. In this study, we analysed the potential of different survey techniques to analyse hazards of the Forni glacier, an important geosite located in Stelvio Park (Italian Alps). We carried out surveys in the 2016 ablation season and compared point clouds generated from an unmanned aerial vehicle (UAV) survey, close range photogrammetry and terrestrial laser scanning (TLS). To investigate the evolution of glacier hazards and evaluate the glacier thinning rate, we also used UAV data collected in 2014 and a digital elevation model (DEM) created from an aerial photogrammetric survey of 2007. We found that the integration between terrestrial and UAV photogrammetry is ideal for mapping hazards related to the glacier collapse, while TLS is affected by occlusions and is logistically complex in glacial terrain. Photogrammetric techniques can therefore replace TLS for glacier studies and UAV-based DEMs hold potential for becoming a standard tool in the investigation of glacier thickness changes. Based on our datasets, an increase in the size of collapses was found over the study period, and the glacier thinning rates went from 4.55 ± 0.24 ma^{-1} between 2007 and 2014 to 5.20 ± 1.11 ma^{-1} between 2014 and 2016.

1 Introduction

Glacier and permafrost-related hazards can be a serious threat to humans and infrastructure in high mountain regions (Carey et al., 2014). The most catastrophic cryospheric hazards are generally related to water outbursts , either through breaching of moraine- or ice-dammed lakes or from the englacial or subglacial system, causing floods and debris flows. Ice avalanches from hanging glaciers can also have serious consequences for downstream populations (Vincent et al., 2015), as well as debris flows caused by the mobilization of accumulated loose sediment on steep slopes (Kaab et al., 2005a). Less severe hazards, but still particularly threatening for mountaineers, are the

35 detachment of seracs (Riccardi et al., 2010) or the collapse of ice cavities (Gagliardini et al., 2011;
36 Azzoni et al., 2017). While these processes are in part typical of glacial and periglacial
37 environments, there is evidence that climate change is increasing the likelihood of specific hazards
38 (Kaab et al., 2005a). In the European Alps, accelerated formation and growth of proglacial moraine-
39 dammed lakes has been reported in Switzerland, amongst concern of possible overtopping of
40 moraine dams provoked by ice avalanches (Gobiet et al., 2014). Ice avalanches themselves can be
41 more frequent as basal sliding is enhanced by the abundance of meltwater in warmer summers
42 (Clague, 2013). Glacier and permafrost retreat, which have been reported in all sectors of the Alps
43 (Smiraglia et al., 2015; Fischer et al., 2014; Gardent et al., 2014; Harris et al., 2009), are a major
44 cause of slope instabilities which can result in debris flows, by debuttressing rock and debris flanks
45 and promoting the exposure of unconsolidated and ice-cored sediments (Keiler et al., 2010; Chiarle
46 et al., 2007). Glacier downwasting causes changes in water resources, with an initial increase in
47 discharge due to enhanced melt followed by a long-term reduction, affecting drinking water supply,
48 irrigation and hydropower production (Kaab et al., 2005b), along with a rising occurrence of
49 structural collapses (Azzoni et al., 2017). Finally, glacier retreat and the increase in glacier hazards
50 both negatively influence the tourism sector and the economic prosperity of high mountain regions
51 (Palomo, 2017).

52 The growing threat from cryospheric hazards under climate change calls for the adoption of
53 mitigation strategies. Remote sensing has long been recognized as an important tool for producing
54 supporting data for this purpose, such as digital elevation models (DEMs) and multispectral images.
55 DEMs are particularly useful for detecting glacier thickness and volume variations (Fischer et al.,
56 2015; Berthier et al., 2016) and for identifying steep areas that are most prone to
57 geomorphodynamic changes, such as mass movements (Blasone et al., 2014). Multispectral images
58 at a sufficient spatial resolution make it possible to recognize most cryospheric hazards (Quincey et
59 al., 2005; Kaab et al., 2005b). While satellite images from Landsat and ASTER sensors (15-30 m

ground sample distance - GSD) are practical for regional-scale mapping (Rounce et al, 2017), the assessment of hazards at the scale of individual glaciers or basins requires a higher spatial resolution, which in the past could only be achieved via aerial laser scanner/photogrammetric surveys (Vincent et al., 2010; Janke, 2013) or dedicated field campaigns with terrestrial laser scanners (TLS) (Kellerer-Pirklbauer et al., 2005; Riccardi et al., 2010). Recent years have seen a resurgence of terrestrial photogrammetric surveys for the generation of DEMs (Piermattei et al., 2015, 2016; Kaufmann and Seier, 2016) due to important technological advances, including the development of Structure-from-Motion (SfM) photogrammetry and its implementation in fully automatic processing software, as well as improvements in the quality of camera sensors (Eltner et al., 2016; Westoby et al., 2012). In parallel, unmanned aerial vehicles (UAVs – Colomina & Molina, 2014, O'Connor et al., 2017) have started to emerge as a viable alternative to TLS for multi-temporal monitoring of small areas. UAVs promise to bridge the gap between field observations, notoriously difficult on glaciers, and coarser resolution satellite data (Bhardwaj et al., 2016). Although the number of studies employing these platforms in high mountain environments is on the rise (see e.g. Fugazza et al., 2015; Gindraux et al., 2017; Seier et al., 2017), their full potential for monitoring glaciers and particularly glacier hazards has yet to be explored. In particular, the advantages of UAV and terrestrial SfM-photogrammetry and the possibility of data fusion and volume change estimation to support hazard management strategies in glacial environments needs to be investigated and assessed.

In this study, we investigated a rapidly downwasting glacier (almost 5 ma^{-1} water equivalent, Senese et al., 2012) in a protected area and highly touristic sector of the Italian Alps, Stelvio National Park. We focused on the glacier terminus and the hazards identified there, i.e., the formation of normal faults and ring faults. The former occur mainly on the medial moraines and glacier terminus and are due to gravitational collapse of debris-laden slopes. The latter develop as a series of circular or semicircular fractures with stepwise subsidence, caused by englacial or subglacial meltwater creating

85 voids at the ice-bedrock interface, eventually leading to the collapse of the cavity roofs. While often
86 overlooked, these collapse structures are particularly hazardous for mountaineers and they are likely to
87 increase under a climate change scenario (Azzoni et al., 2017). They are more dangerous than
88 crevasses because of their larger size.
89 We conducted our first UAV survey of the glacier in 2014; in summer 2016, the glacier was surveyed
90 using three different techniques for the generation of point clouds, DEMs and orthophotos. The
91 aims were: (1) to compare the different methods and select the most appropriate ones for
92 monitoring glacier hazards (2) to identify glacier-related hazards and their evolution between 2014-
93 2016; and 3) to investigate changes in ice thickness between 2014-2016 and 2007-2016 by
94 comparing the two UAV DEMs and a third DEM obtained from stereo-processing of aerial photos
95 captured in 2007.
96
97 **2 Study area**
98 The Forni Glacier (see Fig. 1) has an area of 11.34 km^2 based on the 2007 data from the Italian
99 Glacier Inventory (Smiraglia et al., 2015); an altitudinal range between 2501 and 3673 m a.s.l., and
100 a North-North-Westerly aspect. The glacier has retreated markedly since the little ice age, when its
101 area was 17.80 km^2 (Diolaiuti & Smiraglia, 2010), with an acceleration of the shrinkage rate over
102 the past three decades, typical of valley glaciers in the Alps (Diolaiuti et al., 2012, D'Agata et al.;
103 2014). It has also undergone profound changes in dynamics in recent years, such as the loss of ice
104 flow from the eastern accumulation basin towards its tongue and the evidence of collapsing areas on
105 the eastern tongue (see Fig. 2d; Azzoni et al., 2017). Continuous monitoring of these hazards is
106 important, as the site is highly touristic (Garavaglia et al., 2012). The glacier is in fact frequently
107 visited during both summer and winter months. During the summer, hikers heading to Mount San
108 Matteo take the trail along the central tongue, accessing the glacier through the left flank of the
109 collapsing glacier terminus (see Fig. 2b, c). During wintertime, ski-mountaineers instead access the

glacier from the eastern side, crossing the medial moraine and potentially collapsed areas there (see Fig. 1, 2a).

3 Data sources: acquisition and processing

In this study, we took advantage of a UAV survey performed in 2014 (Fugazza et al., 2015). Then, through a field campaign in 2016, we conducted different surveys using a UAV, terrestrial photogrammetry and TLS. In the 2014 UAV survey, no ground control points (GCPs) were collected, while in 2016 we specifically set up a control network for geo-referencing purposes. Processing of the UAV and terrestrial images was carried out using Agisoft Photoscan version 1.2.4 (www.agisoft.com), implementing a SfM algorithm for image orientation followed by a multi-view dense-matching approach for surface 3D reconstruction (Westoby et al., 2012). In addition, we employed a DEM from an aerial survey of 2007 to calculate glacier thickness changes over a period of 7 to 9 years.

3.1 UAV photogrammetry

3.1.1 2014 Dataset

The first UAV survey took place on 28th August 2014, using a SwingletCam fixed wing aircraft (see Fig. 3a). This commercial platform developed by SenseFly carries a Canon Ixus 127 HS compact digital camera. The UAV was flown in autopilot mode with a relative flying height of approximately 380 m above the glacier surface, which resulted in an average GSD of 12 cm. The flight plan was organized by using the proprietary software eMotion, by which the aircraft follows predefined waypoints with a nominal along-strip overlap of 70%. In our study, sidelap was not regular because of the varying surface topography, but it averaged approximately 60%. Flight operations started around 07:30 AM and ended around 08:30 AM. Early morning operations were preferred to avoid saturating camera pictures, as during this time of day the glacier is not yet directly illuminated by the sun, and to minimize blurring effects due to the UAV motion, since wind speed is at its lowest on glaciers during morning hours (Fugazza et al., 2015). Pictures were automatically captured by

135 the UAV platform, selecting the best combination of sensor aperture (F=2.7), sensitivity (between
136 100-400 ISO) and shutter speed (between 1/125 s - 1/640 s). The survey covered an area of 2.21
137 km^2 in two flight campaigns, with a low altitude take-off (see Fig. 1). Both the terminal parts of the
138 central and eastern ablation tongue were surveyed.

139 Since no GCPs were measured during the 2014 campaign, the registration of this data set into the
140 mapping reference system was based on GNSS (Global Navigation Satellite System) navigation
141 data only. Consequently, a global bias in the order of 1.5-2 m resulted after geo-referencing, and no
142 control on the intrinsic geometric block stability was possible. After the generation of the point
143 cloud, a DEM and orthophoto were produced with spatial resolutions of 60 cm and 15 cm,
144 respectively.

145 **3.1.2 2016 Dataset**

146 Two UAV surveys were carried out on 30th August and 1st September 2016, both around midday
147 with 8/8 of the sky covered by stratocumulus clouds. The UAV employed in these surveys was a
148 customized quadcopter (see Fig. 3b) carrying a Canon Powershot 16 Megapixel digital camera. Two
149 different take-off and landing sites were chosen to gain altitude before take-off and maintain line-of-
150 sight operation with a flying altitude of 50 m above ground, which ensured an average ground
151 sample distance (GSD) of 6 cm. To reduce motion blur, camera shutter speed was set to the lowest
152 possible setting, 1/2000 s, with aperture at F/2.7 and sensitivity at 200 ISO.

153 Several flights were conducted to cover a small section of the proglacial plain and different surface
154 types on the glacier surface, including the terminus, a collapsed area on the central tongue, the
155 eastern medial moraine and some debris-covered parts of the eastern tongue. A ‘zig-zag’ flying
156 scheme was followed to reduce the flight time. The UAV was flown in autopilot mode using the
157 open-source software Mission Planner (Oborne, 2013) to ensure 70% along-strip overlap and

158 sidelap. In total, two flights were performed during the first survey and three during the second,
159 lasting about 20 minutes each. The surveyed area spanned over 0.59 km^2.

160 Eight GCPs (see Fig. 1) were measured for the registration of the photogrammetric blocks and its
161 by-products into the mapping system. The root mean square error (RMSE) of the GCP location was
162 40 cm, which can be used as an indicator of the internal consistency of the photogrammetric block.
163 The point cloud obtained from the 2016 UAV flight was interpolated to produce a DEM and
164 orthophoto with the same cell resolution as the 2014 dataset, i.e., 60 and 15 cm, respectively. Both
165 products were exported in the ITRS2000 / UTM 32N mapping reference system.

166 **3.2 Terrestrial photogrammetry**

167 The terrestrial photogrammetric survey was carried out on 29th August 2016 to reconstruct the
168 topographic surface of the glacier terminus, which presented several vertical and subvertical
169 surfaces (see Fig. 2e) whose measurement was not possible from the UAV platform carrying a
170 camera in nadir configuration.

171 Images were captured from 134 ground-based stations, most of them located in front of the glacier,
172 and some on both flanks of the valley in the downstream area. A single-lens-reflex Nikon D700
173 camera was used, equipped with a 50 mm lens, and a full-frame CMOS sensor (36x24 mm) with
174 4256x2823 pixels. In this case, since no preliminary information about approximate camera position
175 was collected, the SfM procedure was run without any initial information.

176 Seven natural features visible on the glacier front were used as GCPs to be included in the bundle
177 adjustment computation. Measurement of GCPs in the field was carried out by means of a high-
178 precision theodolite. The measurement of points previously recorded with a GNSS geodetic
179 receiver made it possible to register the coordinates of GCPs in the mapping reference system. The
180 RMSE of 3D residual vectors on GCPs was 34 cm.

3.3 Terrestrial Laser Scanning

On the same days as the first UAV survey of 2016, a long-range terrestrial laser scanner Riegl LMS-Z420i was used to scan the glacier terminus. One instrumental standpoint located on the hydrographic left flank of the glacier terminus (see Fig. 1) was established. The horizontal and vertical scanning resolution were set up to provide a spatial point density of approx. 5 cm on the ice surface at the terminus. Geo-referencing was accomplished by placing five GCPs consisting in cylinders covered by retroreflective paper. The coordinates of GCPs were measured by using a precision theodolite following the same procedure adopted for terrestrial photogrammetry. Considering the accuracy of registration and the expected precision of laser point measurement, the global uncertainty of 3D points was estimated on the order of ±7.5 cm.

3.4 GNSS ground control points

Prior to the 2016 surveys, eight control targets were placed both on the periglacial area and on the glacier tongue (see Fig. 1). Differential GNSS (global navigation satellite system) data were acquired at the target location for the geo-referencing of UAV, terrestrial photogrammetry and TLS data. GCPs were used 1) to geo-reference UAV data directly, by identifying the targets on the images in Photoscan; 2) to register theodolite measurements for geo-referencing terrestrial photogrammetry and TLS. The targets consisted in a square piece of white fabric (80 x 80 cm), with a circular marker in red paint chosen to provide contrast against the background. Except for the one GCP located at the highest site, such GCPs were positioned on large, flat boulders to provide a stable support and reduce the impact of ice ablation between flights.

GNSS data were acquired by means of a pair of Leica Geosystems 1200 geodetic receivers working in RTK (Real-Time Kinematics) mode (see Hoffman-Wellenhof, 2008). One of them was set up as master on a precise point beside Branca hut, with known coordinates in the mapping reference system ITRS2000 / UTM 32N. The second receiver was used as a rover, communicating via radio

link with the master station. The maximum distance between master and rover was less than 1.5 km, but due to the local topography preventing the radio link and the lack of mobile phone services (for RTK), some points were measured in static mode with measurement time of approximately 12 minutes. The theoretical uncertainty of GCPs provided by the processing code was on the order of 2-3 cm.

3.5 2007 DEM

The 2007 TerraItaly DEM was produced by the BLOM C.G.R. company for the Lombardy region. It is the final product of an aerial survey over the entire region, conducted with a multispectral pushbroom Leica ADS40 sensor acquiring images from a flying height of 6,300 m with an average GSD of 65 cm. The images were processed to generate a DEM with a cell resolution of 2 m x 2 m, and a ±3 m uncertainty. We converted the DEM from the "Monte Mario" to the "ITRS2000" datum and the height from ellipsoidal to geodetic using the official software for datum transformation in Italy (Verto ver. 3).

4 Methods

4.1 Analysis of point clouds from the 2016 campaign: UAV/terrestrial photogrammetry and TLS

The comparison between point clouds generated during the 2016 campaign had the aim of assessing their geometric quality before their application for the analysis of hazards. These evaluations were also expected to provide some guidelines for the organization of future investigations in the field at the Forni Glacier and in other Alpine sites. Specifically, we analysed point density (points/m^2) and completeness, i.e. % of area in the ray view angle. Point density partly depends upon the surveying technique used, since it is controlled by the distance between sensor and surface, and determines spatial resolution. In SfM-photogrammetry, point density is affected by image texture, sharpness and resolution, which influence the performance of dense matching algorithms (Dall'Asta et al., 2015), while in TLS it can be set up as a data acquisition input parameter. In this study, the number

of neighbours N (inside a sphere of radius R=1 meter) divided by the neighbourhood surface was used to evaluate the local point density D in CloudCompare (www.cloudcompare.org). To understand the effect of point density dispersion (Teunissen, 2009), the inferior 12.5 percentile of the standard deviation σ of point density was also calculated. The use of these local metrics allowed us to distinguish between point densities in different areas, since this may largely change from one portion of surface to another. A further metric in this sense was point cloud completeness, referring to the presence of enough points to completely describe a portion of surface. In this study, the visual inspection of selected sample locations was used to identify occlusions and areas with lower point density.

To analyse these properties, five regions were selected (see Fig. 4), located on the glacier topographic surface and characterized by different glacier features and the presence of hazards: 1) a glacial cavity composed of subvertical and fractured surfaces over 20 m high, and forming a typical semicircular shape; 2) a glacial cavity over 10 m high with the same typical semi-circular shape as location 1, covered by fine- and medium-sized rock debris; 3) a normal fault over 10 m high; 4) a highly-collapsed area covered by fine- and medium-sized rock debris and rock boulders; and 5) a planar surface with a normal fault covered by fine- and medium-sized rock debris and rock boulders. The analysis of local regions was preferred to the overall analysis of all the point clouds for the following reasons: 1) the incomplete overlap between point clouds obtained from different methods; 2) the opportunity to investigate the performances of the techniques in diverse geomorphological situations.

Within the same sample locations, we compared the point clouds in a pairwise manner. Since no available benchmarking data set (e.g. accurate static GNSS data) was concurrently collected during the 2016 campaign, the TLS point cloud was used as a reference. When comparing both photogrammetric data sets, the one obtained from the UAV was used as reference because of the even distribution of point density within the sample locations. The presence of residual, non-

255 homogenous geo-referencing errors in the data sets required a specific fine registration of each
256 individual sample location, which was conducted in CloudCompare using the ICP (iterative closest
257 point) algorithm (Pomerleau et al., 2013). ICP iteratively matches a source point cloud to a
258 reference point cloud in Euclidean space and calculates the necessary rotation and translation to
259 align the source point cloud with the reference based on minimization of a distance metric in a
260 point-to-point fashion. After fine registration, point clouds in corresponding sample areas were
261 compared using the M3C2 algorithm implemented in CloudCompare (Lague et al., 2013). As
262 discussed in Fey and Wichmann (2016), the distance between a pair of point clouds is often
263 evaluated by comparing elevations at corresponding nodes of DEMs, after resampling of the
264 original data. This approach works properly when both point clouds are approximately aligned
265 along the same planar direction, but not when there are structures with different alignments as in the
266 case of the glacier surfaces under investigation. In fact, the M3C2 algorithm does not always
267 evaluate the distance between two point clouds along the same directional axis, but computes a set
268 of local normals using points within a radius D depending on the local roughness, which is directly
269 estimated from the point cloud data, and also considering the uncertainty of preliminary local
270 registration refinement using ICP. In this case, a radius D=20 cm and a pre-registration uncertainty
271 of 5 cm were considered, the latter obtained from ICP residuals. This solution allowed us to
272 remove registration errors from the analysis, and focus on the capability of the adopted techniques
273 to reconstruct the local geometric surface of the glacier in an accurate way.

274 **4.2 Point cloud merging**

275 To improve coverage of different glacier surfaces, including planar areas and normal faults,
276 photogrammetric point clouds from the 2016 campaign (UAV and terrestrial surveys) were merged.
277 We chose to avoid TLS and employed the two lower cost techniques (Chandler and Buckley, 2016)
278 to assess their potential for combined future use. Prior to point cloud merging, a preliminary co-
279 registration was performed on the basis of the ICP algorithm in CloudCompare. Regions common to

both point clouds were used to minimize the distances between them and find the best co-registration. The point cloud from UAV photogrammetry, which featured the largest extension, was used as reference during co-registration, while the other was rigidly transformed to fit with it. After many iterations, both point clouds were aligned according to the best solution found by the ICP. In order to remove redundant points and to obtain a homogenous point density, the merged point cloud (see Fig. 5) was subsampled keeping a minimum distance between adjacent points of 20 cm. The final size of this merged data set is approximately 4.4 million points. The RGB colour information associated with each point in the final point cloud was derived by averaging the RGB information of original points in the subsampling volumes. While this operation resulted in losing part of the original RGB information, it helped to provide a realistic visualization of the topographic model, and therefore to interpret glacier hazards.

4.2 Glacier hazard mapping

The investigation of glacier hazards was conducted using the point cloud and orthophoto from the 2014 UAV dataset as well as the merged (UAV and terrestrial) point cloud and orthophoto from 2016. In this study, we focused on ring faults and normal faults, which were identified by visually inspecting their geometric properties in the point clouds and manually delineated, while colour information from orthophotos was used as a cross-check. On orthophotos, both types of structures generally appear as dark linear features owing to shadows projected by fault scarps. As these structures may look similar to crevasses, further information concerning their orientation and location needs to be assessed for discrimination. The orientation of fault structures is not coherent with glacier flow, with ring faults also appearing in circular patterns. Their location is limited to the glacier margins, medial moraines and terminus, whereas crevasses can appear anywhere on the glacier surface (Azzoni et al., 2017). After delineation, we also analysed the height of vertical facies using information from the point clouds.

4.3 DEM Co-registration for glacier thickness change estimation

Several studies have found that errors in individual DEMs, both in the horizontal and vertical domain, propagate when calculating their difference, leading to inaccurate estimations of thickness and volume change (Berthier et al., 2007; Nuth & Kaab, 2011). In the present study, different approaches were adopted for geo-referencing all the DEMs used in the analysis of the volume change of the Forni Glacier tongue (2007, 2014, 2016). To compute the relative differences between the DEMs, a preliminary co-registration was therefore required. The method proposed by Berthier et al. (2007) for the co-registration of two DEMS was separately applied to each DEM pair (2007-2014; 2007-2016; 2014-2016). Following this method, in each pair one DEM plays as reference ('master'), while the other is used as 'slave' DEM to be iteratively shifted along x and y axes by fractions of a pixel to minimize the standard deviation of elevation differences with respect to the 'master' DEM. Only areas assumed to be stable are considered in the calculation of the co-registration shift. The ice-covered areas were excluded by overlaying the glacier outlines from D'Agata et al. (2014) for 2007 and Fugazza et al. (2015) for 2014. The oldest DEM, which is also the widest in each comparison, was always set as the master. To co-register the 2014 and 2016 DEMs with the 2007 DEM, both were resampled to 2 m spatial resolution, whereas the comparison between 2014 and 2016 was carried out at the original resolution of these data sets (60 cm).

All points resulting in elevation differences greater than 15 m were labelled as unreliable, and consequently discarded from the subsequent analysis. Such greater discrepancies may denote errors in one of the DEMs or unstable areas outside the glacier. Values exceeding this threshold, however, were only found in a marginal area with low image overlap in the comparison between the 2014 and 2016 DEMs, with a maximum elevation difference of 36 m. Once the final co-registration shifts were computed (see Table 1), the coefficients were subtracted from the top left coordinates of the 'slave' DEM; the residual mean elevation difference was also subtracted from the 'slave' DEM to bring the mean to zero. After DEM co-registration, the resulting shifts reported in Table 1 were applied to each 'slave' DEM, including the entire glacier area. Then the elevations of the 'slave'

330 DEM were subtracted from the corresponding elevations of the 'master' DEM to obtain the so-
331 called DEM of Differences (DoD). Over a common glacier area (Fig. 1), we estimated the volume
332 change and its uncertainty, which can be expressed as the combination of 1) uncertainty due to
333 errors in elevation and 2) the truncation error caused by the use of a discrete sum (sum of DoD at
334 each pixel multiplied by pixel area) in place of the integral in volume calculation (Jokinen and
335 Geist, 2010). We calculated the former following the approach of Rolstad et al. (2009), taking into
336 account spatial autocorrelation of elevation change over stable areas, considering a correlation
337 length of 50 m; for the latter, we used the method described by Jokinen and Geist (2010).

338 **5 Results**

339 **5.1 Point cloud Analysis**

340 The analysis of point density shows significant differences between the three techniques for point
341 cloud generation (see Table 2). Values range from 103 to 2297 points/m^2 depending on the
342 surveying method, but the density was generally sufficient for the reconstruction of the different
343 surfaces shown in Fig. 4, except for location 5. Terrestrial photogrammetry featured the highest
344 point density, while UAV photogrammetry had the lowest. In relation to UAV photogrammetry,
345 similar point densities were found in all sample locations, especially for the standard deviations that
346 were always in the 22-29 point/m^2 range. Mean values were 103-109 points/m^2 in locations 2-4,
347 while they were higher in location 5 (141 points/m^2). Due to the nadir acquisition points, the 3D
348 modelling of vertical/sub-vertical cliffs in location 1 was not possible. In relation to TLS, a mean
349 value of point density ranging from 141-391 points/m^2 was found, with the only exception of
350 location 5, where no sufficient data were recorded due to the position of this region with respect to
351 the instrumental standpoint. Standard deviations ranged between 69-217 points/m^2, moderately
352 correlated with respective mean values. The analysis of the completeness of surface reconstruction
353 also revealed some issues related to the adopted techniques (see Fig. 5). Specifically, TLS suffered
354 from severe occlusions, which prevented acquisition of data in the central part of the sample area,

355 while UAV photogrammetry was able to reconstruct the upper portion of the sample area but not the
356 vertical cliff. Only terrestrial photogrammetry acquired a large number of points in all areas.

357 In terms of point cloud distance (see Table 3), the comparison between TLS and terrestrial
358 photogrammetry resulted in a high similarity between point clouds, with no great differences
359 between different sample areas. Conversely, the comparison between TLS and UAV
360 photogrammetry and terrestrial and UAV photogrammetry provided significantly worse results,
361 which may be summarized by the RMSEs in the range 21.1-37.7 cm and 20.7-30.4 cm, respectively.
362 The greater deviations were in both cases obtained in the analysis of location 2, which mostly
363 represents a vertical surface, while the best agreement was found within location 3 which is less
364 inclined. As the UAV flight was geo-referenced on a set of GCPs with an RMSE of 40.5 cm, the
365 ICP co-registration may have not totally compensated the existing bias.

366 In terms of spatial coverage, considering the entire surface examined using each technique outside
367 the sample locations, the UAV survey extended over the widest area (0.59 km^2), including part of
368 the proglacial plain, the entire terminus and the glacier tongue up to the collapsed area on the
369 central part, but with data gaps on the vertical and sub-vertical walls (see Fig. 6a). The point cloud
370 obtained from terrestrial photogrammetry covered approximately a third of the area surveyed with
371 the UAV (see fig. 6b), including the full glacier terminus at very high spatial resolution, with the
372 exception of a few obstructed parts, while the TLS point cloud covered the terminus, although with
373 some holes due to the obstructions.

374 **5.2 Glacier-related hazards and risks**

375 The tongue of Forni glacier hosts a variety of hazardous structures. While most collapsed areas are
376 normal faults, two large ring fault systems can be identified: the first, located in the eastern section
377 (see Fig. 2d and Fig. 7), covered an area of 25.6×10^3 m^2 and showed surface dips of up to 5 m in
378 2014. This area was not surveyed in 2016, since field observation did not show evidence of further
379 subsidence. Conversely, the ring fault that only emerged as a few semi-circular fractures in 2014

grew until cavity collapse, with a vertical displacement up to 20 m and further fractures extending south-eastward (see Fig. 2c and Fig. 7), thus potentially widening the extent of collapse in the future. Further smaller ring faults were identified in 2014 at the eastern glacier margin. Only one of them was included in the area surveyed in 2016, with further 2 m subsidence and an increase in subparallel fractures.

Normal faults are mostly found on the eastern medial moraine and at the terminus. Between 2014 and 2016, the first (see Fig. 2a) developed rapidly in the vertical domain reaching a height of 12 m in 2016. The collapse was even more rapid at the terminus, leading to the formation of three sub-vertical facies, up to 24 m high (see Fig. 2b and 2e), while the height of the vault is as low as 10 m. Several fractures also appear in conjunction with the large ring fault located in the central section of the glacier, extending the fracture system to the western glacier margin. It is likely that the terminus will recede along the fault system on the eastern medial moraine and following the ring faults at the eastern and western margins, increasing the occurrence of hazardous phenomena in these areas.

5.3 Glacier thickness change

The Forni Glacier tongue was affected by substantial thinning throughout the observation period. Between 2007 and 2014, the greatest thinning occurred in the eastern section of the glacier tongue, with changes persistently lower than –30 m (more than 4 ma^{-1} thinning), whereas the upper part of the central tongue only thinned by 10/18 m (between approximately 1 and 2.5 ma^{-1}). The greatest ice loss occurred in correspondence with the normal faults localized in small areas at the eastern glacier margin (see Fig. 8a), with local changes generally lower than -50 m (more than 7 ma^{-1} thinning) and a minimum of -66.80 m, owing to the formation of a lake. Conversely, between 2014 and 2016 the central and eastern parts of the tongue had similar thinning patterns, with average changes of -10 m (5 ma^{-1}). The greatest losses are mainly found in correspondence with normal faults, with a maximum change of -38.71 m at the terminus and local thinning greater than 25 m on

404 the lower medial moraine. The ring fault at the left margin of the central section of the tongue also
405 shows thinning of 20 to 26 m (10-13 ma^{-1}). In the absence of faults, little thinning occurred instead
406 on the upper part of the medial moraine, where a thick debris cover shielded ice from ablation, with
407 changes of -2 to -5 m (1 to 2.5 ma^{-1}, see Fig. 8c). Considering a common reference area (see Fig. 1,
408 table 4), an acceleration of glacier thinning seems to have occurred over recent years over the lower
409 glacier tongue, from -4.55 ± 0.24 ma^{-1} in 2007-2014 to -5.20 ± 1.11 ma^{-1} in 2014-2016, also
410 confirmed by the value of -4.76 ± 0.29 ma^{-1} obtained from the comparison between 2007 and 2016.
411 Looking at the first two DoD, the trend seems to be caused by the increase in collapsing areas
412 (Fig.8a,b). In all DoDs, the uncertainty in ice thickness change affects less than 3% of the respective
413 volume change (see Table 4).
414

415 **6 Discussion: comparison of techniques for point cloud generation**

416 The choice of a technique to monitor glacier hazards and the glacier thickness changes depends on
417 several factors, including the size of the area, the desired spatial resolution and accuracy, logistics
418 and cost. In this study, we focused on spatial metrics, i.e. point density, completeness and distance
419 between point clouds to evaluate the performance of UAV, close-range photogrammetry and TLS in
420 a variety of conditions.

421 **6.1 Point density and completeness**

422 Considering point density, terrestrial photogrammetry resulted in a denser data set than the other
423 techniques. This is mostly motivated by the possibility of acquiring data from several stations using
424 this methodology, depending only on the terrain accessibility, reducing the effect of occlusions with
425 a consequently more complete 3D modelling. However, the mean point density achieved when
426 using terrestrial photogrammetry is highly variable, both between different sample locations, and
427 within each location as shown by the standard deviations of *D*. Point densities related to UAV

428 photogrammetry and TLS are more regular and constant. In the case of UAV photogrammetry, the
429 homogeneity of point density might be due to the regular structure of the airborne photogrammetric
430 block. In the case of TLS, the regularity is motivated by the constant angular resolution adopted
431 during scanning. Since any technique may perform better when the surface to survey is
432 approximately orthogonal to the sensor's point of view, terrestrial photogrammetry is more
433 efficient for reconstructing vertical and subvertical cliffs (Sample areas 1 and 2) and high-sloped
434 surfaces (Sample areas 3 and 4). On the contrary, airborne UAV photogrammetry provided the best
435 results in location 5 which is less inclined and consequently could be well depicted in vertical
436 photos. In general, point clouds from terrestrial photogrammetry provide a better description of the
437 vertical and subvertical parts (see e.g. Winkler et al., 2012), while point clouds obtained from UAV
438 photogrammetry are more suitable to describe the horizontal or sub-horizontal surfaces on the
439 glacier tongue and periglacial area (Seier et al., 2017), unless the camera is tilted to an off-nadir
440 viewpoint (Dewez et al., 2016; Aicardi et al., 2016). Results obtained from photogrammetry based
441 on terrestrial and UAV platforms can thus be considered quite complementary and they support the
442 concept of merging the point clouds from these two techniques, as seen in Fig. 6c. In agreement
443 with other studies of vertical rock slopes (e.g. Abellan et al., 2014), we found that the TLS point
444 cloud was affected by occlusions (see e.g. location 2 in Fig. 4, 5), which can only be compensated
445 by increasing the number of stations. Data acquisition with this platform was in general difficult in
446 regions subparallel to the laser beams and in the presence of wet surfaces.

447 **6.2 Point cloud and DEM uncertainty**

448 In this study, the distance between the UAV and TLS point clouds (21.1-37.7 cm RMSE), assumed
449 as a measure of the uncertainty of the 2016 UAV dataset, was slightly higher than previously
450 reported in high mountain glacial environments (e.g. Immerzeel et al., 2014; Gindraux et al., 2017
451 and Seier et al., 2017), although in these studies the comparison was between DEMs and GNSS
452 control points. Contributing factors might include the sub-optimal distribution and density of GCPs

453 (Gindraux et al., 2017), the delay between the UAV surveys as well as between the UAV and TLS,
454 and the lack of coincidence between GCP placement and the UAV flights. This means the UAV
455 photogrammetric reconstruction was affected by ice ablation and glacier flow, which on Forni
456 Glacier range between 3 and 5 cm day^{-1} (Senese et al., 2012) and 1-4 cm day^{-1}, respectively (Urbini
457 et al., 2017). We thus expect a combined 3-day uncertainty on the 2016 UAV dataset between 10
458 and 20 cm, and lower on GCPs considering reduced ablation owing to their placement on boulders.
459 A further contribution to the GCP error budget might stem from the intrinsic precision of
460 GNSS/theodolite measurements and image resolution. The comparison between close-range
461 photogrammetry and TLS was less affected by glacier change as data were collected one day apart
462 and the RMSE of 6-10.6 cm is in line with previous findings by Kaufmann and Landstaedter
463 (2008). To reduce the uncertainty of UAV photogrammetric blocks, a better distribution of GCPs or
464 switching to an RTK system should be considered, while close-range photogrammetry could benefit
465 from measuring a part of the photo-stations as proposed in Forlani et al. (2014), instead of placing
466 GCPs on the glacier surface.

467 The uncertainty in UAV photogrammetric reconstruction also factored in the standard deviation still
468 present after the co-registration between DEMs in areas outside the glacier (2.22 m between 2014
469 and 2016). Another important factor here is the morphology of the co-registration area, i.e. the
470 outwash plain, still subject to changes owing to the inflow of glacier meltwater and sediment
471 reworking. UAV photogrammetric products permitted us to investigate ice volume changes over 2
472 years with an uncertainty of 2.60%, while the integration with close-range photogrammetry was
473 required to investigate hazards related to the collapse of the glacier terminus.

474 **6.3 Logistics and costs**

475 In our surveys, it became evident that the main disadvantage of TLS compared to photogrammetry
476 is the complexity of instrument transport and setup. In terms of logistics and workload, up to five

people were involved in the transportation of the TLS instruments (laser scanner, theodolite, at least two topographic tripods and poles, electric generator and ancillary accessories) while two people were required for UAV and close-range photogrammetric surveys, which were also considerably faster. Meteorological conditions and the limited access to unstable areas close to the glacier terminus also prevented the acquisition of TLS data from other viewpoints as done with photogrammetry. Concerning UAV surveys, we conducted them under different meteorological scenarios, and obtained adequate results in early-morning operations with 0/8 cloud cover and midday flights with 8/8 cloud cover. Both scenarios can provide diffuse light conditions allowing collection of pictures suitable for photogrammetric processing, but camera settings need to be carefully adjusted beforehand (O'Connor et al., 2017). If early morning flights are not feasible in the study area for logistical reasons or when surveying glaciers with eastern exposures, the latter scenario should be considered.

In terms of costs, UAV and terrestrial photogrammetric surveys are also advantageous, since TLS instruments are much more expensive at €70,000-100,000 compared to UAVs (€3500 for our platform) and DSLR (Digital Single-Lens Reflex) cameras used in photogrammetry, in the €500-3500 range.

6.4 Additional remarks

In summary, although TLS point clouds are regarded as the most accurate (Naumann et al., 2013), they suffer from inhomogeneous point density and cumbersome logistics, and their potential in glacial environments is limited, unless a maximum uncertainty of 5-10 cm can be tolerated. Laser scanners are also employed on aerial platforms, including UAVs, where they can reconstruct terrain morphology with only slightly higher uncertainty than the terrestrial counterparts with a much greater coverage (Raymond et al., 2009), but the high operational cost has limited the diffusion of this technique. Lastly, photogrammetry from higher altitude aerial platforms (mostly planes, but

501 also helicopters and satellites) can similarly achieve low uncertainty (3 m, Andreassen et al., 2002)
502 and extensive coverage at the price of a lower spatial resolution compared to UAVs (e.g. 2 m in our
503 case), and due to its popularity in the past it is often the only means to acquire good quality archive
504 data to investigate glacier changes over broad time scales (Andreassen et al., 2002; Molg et al.,
505 2017).

506 In our pilot study, we covered part of the Forni glacier tongue, and investigated different techniques
507 to map/monitor hazards related to the glacier collapse. Our maps can help identify safer paths where
508 mountaineers and skiers can visit the glacier and reach the most important summits. However, the
509 increase in collapse structures owing to climate change requires multi-temporal monitoring. A
510 comprehensive risk assessment should also cover the entire glacier, to investigate the probability of
511 serac detachment and provide an estimate of the glacier mass balance with the geodetic method.
512 While our integrated approach using a multicopter and terrestrial photogrammetry should be
513 preferred to TLS for the investigation of small individual ice bodies, fixed-wing UAVs, ideally
514 equipped with an RTK system and the ability to tilt the camera off-nadir, might be the platform of
515 choice to cover large distances (see e.g. Ryan et al., 2017), potentially reducing the number of
516 flights and solving issues with GCP placement. Such platforms could help collect sufficient data for
517 hazard management strategies up to the basin scale in Stelvio National Park and other sectors of the
518 Italian Alps, eventually replacing higher altitude aerial surveys. Cost analyses (Matese et al., 2015)
519 should also be performed to evaluate the benefits of improved spatial resolution and lower DEM
520 uncertainty of UAVs compared to aerial and satellite surveys and choose the best approach for
521 individual cases.

522 **7 Conclusions**

523 In our study, we compared point clouds generated from UAV photogrammetry, close-range
524 photogrammetry, and TLS to assess their quality and evaluate their potential in mapping and

describing glacier hazards such as ring faults and normal faults, in a specific campaign carried out in summer 2016. In addition, we employed orthophotos and point clouds from a UAV survey conducted in 2014 to analyse the evolution of glacier hazards, as well as a DEM from an aerial photogrammetric survey conducted in 2007, to investigate glacier thickness changes between 2007 and 2016. The main findings of our study include:

- UAVs and terrestrial photogrammetric surveys provide reliable performances in glacial environments and outperform TLS in terms of logistics and costs.
- UAV and terrestrial photogrammetric blocks can be easily integrated providing more information than individual techniques to help identify glacier hazards.
- UAV-based DEMs can be employed to estimate thickness and volume changes but improvements are necessary in terms of area covered and to reduce uncertainty.
- The Forni Glacier is rapidly collapsing with an increase in ring fault sizes, providing evidence of climate change in the region.
- The glacier thinning rate increased owing to collapses to 5.20±1.11 ma^{-1} between 2014 and 2016.

The maps produced from the combined analysis of UAV and terrestrial photogrammetric point clouds and orthophotos can be made available through GIS web portals of the Stelvio National Park or the Lombardy region (http://www.geoportale.regione.lombardia.it/). A permanent monitoring programme should be set up to help manage risk in the area, issuing warnings and assisting mountain guides in changing hiking and ski routes as needed. The analysis of glacier thickness changes suggests a feedback mechanism which should be further analysed, with higher thinning rates leading to increased occurrence of collapses. Glacier downwasting is also of relevance for risk management in the protected area, providing valuable data to assess the increased chance of rockfalls and to improve forecasts of glacier meltwater production.

While our test was conducted on one of the largest glaciers in the Italian Alps, the integrated photogrammetric approach is easily transferable to similar sized and much smaller glaciers, where it would be able to provide a comprehensive assessment of hazards and thickness changes and become useful in decision support systems for natural hazard management. In larger regions, UAVs hold the potential to become the platform of choice, but their performances and cost-effectiveness compared to aerial and satellite surveys need to be further evaluated.

Competing interests

The authors declare that they have no conflict of interest.

Acknowledgements

This study was funded by DARAS, the Department for Autonomies and Regional Affairs of the Italian government's Presidency of the Council of Ministers. The authors are grateful to the central scientific committee of CAI (Club Alpino Italiano – Italian Alpine Club) and Levissima San Pellegrino S.P.A. for funding the UAV quadcopter. The authors also thank Stelvio Park Authority for the logistic support and for permitting the UAV surveys and IIT Regione Lombardia for the provision of the 2007 DEM. Our gratitude also goes to the GICARUS lab of Politecnico Milano at Lecco Campus for providing the survey equipment. Finally, the authors would also like to thank Tullio Feifer, Livio Piatta, and Andrea Grossoni for their help during field operations.

References

Abellán, A., Oppikofer, T., Jaboyedoff, M., Rosser, N. J., Lim, M. and Lato, M. J.: Terrestrial laser scanning of rock slope instabilities. Earth Surface Processes and Landforms, 39, 80–97, 2014, doi:10.1002/esp.3493.

Aicardi, I., Chiabrando, F.,Grasso, N., Lingua, A.M., Noardo, F. and Spanò, A.: UAV photogrammetry with oblique images: first analysis on data acquisition and processing, International Archives of the Photogrammetry, Remote Sensing and Spatial Information Sciences, Prague, Czech Republic, 12–19 July 2016, 41-B1, 835-842, 2016, doi: 10.5194/isprs-archives-XLI-B1-835-2016.

Andreassen, L.M., Hallgeir, E. and Kjollmoen, B.: Using aerial photography to study glacier changes in Norway, Annals of Glaciology, 34, 343-348, 2010, doi: 10.3189/172756402781817626

577 Azzoni, R.S., Fugazza, D., Zennaro, M., Zucali, M., D'Agata, C., Maragno, D., Cernuschi, M.,
578 Smiraglia, C. and Diolaiuti, G.A.: Recent structural evolution of Forni Glacier tongue (Ortles-
579 Cevedale Group, Central Italian Alps). Journal of Maps, 13, 870-878, 2017, doi:
580 10.1080/17445647.2017.1394227

581 Berthier, E., Arnaud, Y., Kumar, R., Ahmad, S., Wagnon, P. and Chevallier, P.: Remote sensing
582 estimates of glacier mass balances in the Himachal Pradesh (Western Himalaya, India), Remote
583 Sensing of Environment, 108, 327-338, 2007, doi: 10.1016/j.rse.2006.11.017.

584 Berthier, E., Cabot, V., Vincent, C. and Six, D.: Decadal Region-Wide and Glacier-Wide Mass
585 Balances Derived from Multi-Temporal ASTER Satellite Digital Elevation Models.Validation over
586 the Mont-Blanc Area, Frontiers in Earth Science, 4, 63, 2016, doi: 10.3389/feart.2016.00063.

587 Bhardwaj, A., Sam, L., Akanksha, Martin-Torres, F.J. and Kumar, R.: UAVs as remote sensing
588 platform in glaciology: Present applications and future prospects, Remote Sensing of Environment,
589 175, 196-204, 2016, doi: 10.1016/j.rse.2015.12.029.

590 Blasone, G., Cavalli, M. and Cazorzi, F.: Debris-Flow Monitoring and Geomorphic Change
591 Detection Combining Laser Scanning and Fast Photogrammetric Surveys in the Moscardo
592 Catchment (Eastern Italian Alps), in: Lollino, G., Arattano, M., Rinaldi, M., Giustolisi, O.,
593 Marechal, J.C. and Grant, G. (eds) Engineering Geology for Society and Territory, 3, Springer,
594 Cham, 51-54, 2015, doi: 10.1007/978-3-319-09054-2_10.

595 Carey, M., McDowell, G., Huggel, C., Jackson, M., Portocarrero, C., Reynolds, J.M. and Vicuña,
596 L.: Integrated approaches to adaptation and disaster risk reduction in dynamic sociocryospheric
597 systems, in: Haeberli, W. and Whiteman, C. (Eds.), Snow and Ice-related Hazards, Risks and
598 Disasters, Elsevier, 219-261, 2014, doi: 10.1016/B978-0-12-394849-6.00008-1.

599 Chandler, J.H. and Buckley, S.: Structure from motion (SFM) photogrammetry vs terrestrial laser
600 scanning. In: Carpenter, M.B. and Keane, C.M. (eds.) Geoscience Handbook 2016, AGI Data
601 Sheets, 5th ed. Alexandria, US, American Geosciences Institute, Section 20.1, 2016.

602 Chiarle, M., Iannotti, S., Mortara, G. and Deline, P.: Recent debris flow occurrences associated with
603 glaciers in the Alps, Global and Planetary Change, 56, 123-136, 2007, doi:
604 10.1016/j.gloplacha.2006.07.003.

605 Clague, J.: Glacier Hazards, in: Bobrowski, P. (Ed.), Encyclopedia of Natural Hazards, Springer,
606 400-405, 2013, doi: 10.1007/978-1-4020-4399-4_156.

607 Colomina, I. and Molina, P.: Unmanned aerial systems for photogrammetry and remote sensing: A
608 review, ISPRS Journal of Photogrammetry and Remote Sensing, 92, 79-97, 2014, doi:
609 10.1016/j.isprsjprs.2014.02.013.

610 D'Agata, C., Bocchiola, D., Maragno, D., Smiraglia, C. and Diolaiuti, G.A.: Glacier shrinkage
611 driven by climate change during half a century (1954–2007) in the Ortles-Cevedale group (Stelvio
612 National Park, Lombardy, Italian Alps), Theoretical and Applied Cimatology, 116, 169-190, 2014,
613 doi: 10.1007/s00704-013-0938-5.

614 Dall'Asta, E., Thoeni, K., Santise, M., Forlani, G., Giacomini, A., Roncella, R.: Network design and
615 quality checks in automatic orientation of close-range photogrammetric blocks, Sensors, 15, 7985-
616 8008, 2015, doi: 10.3390/s150407985

Dewez, T.J.B., Leroux, J. and Morelli, S.: Cliff collapse hazard from repeated multicopter UAV acquisitions: return on experience, The International Archives of the Photogrammetry, Remote Sensing and Spatial Information Sciences, XXIII ISPRS Congress, Prague, Czech Republic, 12–19 July 2016, 41-B5, 805-811, 2016, doi: 10.5194/isprs-archives-XLI-B5-805-2016

Diolaiuti, G.A. and Smiraglia, C.: Changing glaciers in a changing climate: how vanishing geomorphosites have been driving deep changes in mountain landscapes and environments, Géomorphologie : Relief, Processus, Environnement, 2, 131-152, 2010, doi: 10.4000/geomorphologie.7882.

Diolaiuti, G.A., Bocchiola, D., D'Agata, C. and Smiraglia, C.: Evidence of climate change impact upon glaciers' recession within the Italian Alps, Theoretical and Applied Climatology, 109,429-445, 2012, doi: 10.1007/s00704-012-0589-y

Eltner, A., Kaiser, A., Castillo, C., Rock, G., Neugirg, F. and Abellán, A.: Image-based surface reconstruction in geomorphometry – merits, limits and developments. Earth Surface Dynamics, 4, 359-389, 2016, doi: 10.5194/esurf-4-359-2016.

Fey, C. and Wichmann, V.: Long-range Terrestrial laser scanning for geomorphological change detection in alpine terrain - handling uncertainties. Earth Surface Processes and Landforms, 42, 789-802, 2016, doi: 10.1002/esp.4022.

Fischer, M., Huss, M., Barboux, C. and Hoelzle, M.: The new Swiss Glacier Inventory SGI2010: relevance of using high-resolution source data in areas dominated by very small glaciers, Arctic, Antarctic and Alpine Research, 46,933-945, 2014, doi: 10.1657/1938-4246-46.4.933.

Fischer, M., Huss, M. and Hoelzle, M.: Surface elevation and mass changes of all Swiss glaciers 1980–2010, The Cryosphere, 9, 525-540, 2015, doi: 10.5194/tc-9-525-2015

Forlani, G., Pinto, L., Roncella, R. and Pagliari, D.: Terrestrial photogrammetry without ground control points, Earth Science Informatics, 7, 71-81, 2014, doi: 10.1007/s12145-013-0127-1.

Fugazza, D., Senese, A., Azzoni, R.S., Smiraglia, C., Cernuschi, M., Severi, D. and Diolaiuti, G.A.: High-resolution mapping of glacier surface features. The UAV survey of the Forni glacier (Stelvio national park, Italy), Geografia Fisica e Dinamica Quaternaria, 38, 25-33, 2015, doi: 10.4461/GFDQ.2015.38.03.

Garavaglia, V., Diolaiuti, G.A., Smiraglia, C., Pasquale, V. and Pelfini, M.: Evaluating Tourist Perception of Environmental Changes as a Contribution to Managing Natural Resources in Glacierized areas: A Case Study of the Forni Glacier (Stelvio National Park, Italian Alps), Environmental Management, 50, 1125-1138, 2012, doi: 10.1007/s00267-012-9948-9.

Gagliardini, O., Gillet-Chaulet, F., Durand, G., Vincent, C. and Duval, P.: Estimating the risk of glacier cavity collapse during artificial drainage: The case of Tête Rousse Glacier, Geophysical Research Letters, 38, L10505, 2011, doi:10.1029/2011GL047536.

Gardent, M., Rabatel, A., Dedieu, J.-P., Deline, P.: Multitemporal glacier inventory of the French Alps from the late 1960s to the late 2000s, Global and Planetary Change, 120, 24-37, 2014. doi: 10.1016/j.gloplacha.2014.05.004.

655 Gindraux, S., Boesch, R. and Farinotti, D.: Accuracy Assessment of Digital Surface Models from
656 Unmanned Aerial Vehicles' Imagery on Glaciers, Remote sensing, 9, 186, 2-15, 2017,
657 doi:10.3390/rs9020186.

658 Gobiet, A., Kotlarski, S., Beniston, M., Heinrich, G., Rajczak, J., Stoffel, M.: 21st century climate
659 change in the European Alps—A review, Science of The Total Environment, 493, 1138-1151, 2014,
660 doi: 10.1016/j.scitotenv.2013.07.050.

661 Harris, C., Arenson, L.U., Christiansen, H.H., Etzelmueller, B., Frauenfelder, R., Gruber, S.,
662 Haeberli, W., Hauck, C., Hoelzle, M., Humlum, O., Isaksen, K., Kaab, A., Kern-Luetschg, M.,
663 Lehning, M., Matsuoka, N., Murton, J.B., Noetzli, J., Phillips, M., Ross, N., Seppaelae, M.,
664 Springman, S.M. and Vonder Muehll, D.: Permafrost and climate in Europe: Monitoring and
665 modelling thermal, geomorphological and geotechnical responses, Earth-Science Reviews, 92, 117-
666 171, 2009, doi: 10.1016/j.earscirev.2008.12.002.

667 Hoffmann-Wellenhof, B., Lichtenegger, H. and Wasle, E.: GNSS – GPS, GLONASS, Galileo &
668 more, Springer, 2008, doi: 10.1007/978-3-211-73017-1.

669 Immerzeel, W.W., Kraaijenbrink, P.D.A., Shea, J.M., Shrestha, A.B., Pellicciotti, F., Bierkens,
670 M.F.P. and de Jong, S.M.: High-resolution monitoring of Himalayan glacier dynamics using
671 unmanned aerial vehicles, Remote Sensing of Environment, 150,93-103, 2014, doi:
672 10.1016/j.rse.2014.04.025.

673 Janke, J.R.: Using airborne LiDAR and USGS DEM data for assessing rock glaciers and glaciers,
674 Geomorphology, 195, 118-130, doi: 10.1016/j.geomorph.2013.04.036

675 Jokinen, O. and Geist T.: Accuracy aspects in topographical change detection of glacier surface, in:
676 Remote sensing of glaciers, CRC Press/Balkema, Leiden, the Netherlands, 269-283, 2010, doi:
677 10.1201/b10155-15.

678 Kaab, A., Huggel., C., Fischer, L., Guex, S. Paul, F., Roer., I., Salzmann, N., Schlaefli, S., Schmutz,
679 K., Schneider, D., Strozzi, T. and Weidmann, Y.: Remote sensing of glacier- and permafrost-related
680 hazards in high mountains: an overview, Natural Hazards and Earth System Sciences, 5, 527–554,
681 2005a, doi: 10.5194/nhess-5-527-2005.

682 Kaab, A., Reynolds, J.M. and Haeberli, W.: Glacier and Permafrost hazards in high mountains, in:
683 Huber U.M., Bugmann H.K.M., Reasoner M.A. (eds) Global Change and Mountain Regions.
684 Advances in Global Change Research, Springer, Dordrecht, 225-234, 2005b, doi: 10.1007/1-4020-
685 3508-X_23.

686 Kaufmann, V. and Ladstädter, R.: Application of terrestrial photogrammetry for glacier monitoring
687 in Alpine environments, International Archives of the Photogrammetry, Remote Sensing and Spatial
688 Information Sciences, Beijing, China, 37-B8, 813-818, 2008.

689 Kaufmann, V. and Seier, G.: Long-term monitoring of glacier change at Gössnitzkees (Austria)
690 using terrestrial photogrammetry, The International Archives of the Photogrammetry, Remote
691 Sensing and Spatial Information Sciences, XXIII ISPRS Congress, Prague, Czech Republic, 12-19
692 July 2016, 41-B8, 495-502, 2016, doi: 10.5194/isprs-archives-XLI-B8-495-2016

693 Keiler, M., Knight, J. and Harrison, S.: Climate change and geomorphological hazards in the eastern
694 European Alps, Philosophical Transactions of The Royal Society A, 368, 2461–2479, 2010, doi:
695 10.1098/rsta.2010.0047.

Kellerer-Pirklbauer, A., Bauer, A. and Proske, H.: Terrestrial laser scanning for glacier monitoring: Glaciation changes of the Gößnitzkees glacier (Schober group, Austria) between 2000 and 2004, 3rd Symposion of the Hohe Tauern National Park for research in protected areas, castle of Kaprun, Austria, 15-17 September 2005, 97-106, 2005.

Lague, D., Brodu, N., Leroux, J.: Accurate 3D comparison of complex topography with terrestrial laser scanner: application to the Rangitikei canyon (N-Z). Journal of Photogrammetry and Remote Sensing, 82, 10–26, 2013, doi:10.1016/j.isprsjprs.2013.04.009.

Matese, A., Toscano, P., Di Gennaro, S.F., Genesio, L., Vaccari, F.P., Primicerio, J., Belli, C., Zaldei, A., Bianconi, R., Gioli, B.: Intercomparison of UAV, Aircraft and Satellite Remote Sensing Platforms for Precision Viticulture, Remote Sensing, 7, 2971-2990, 2015, doi:10.3390/rs70302971.

Moelg, N. and Bolch, T.: Structure-from-Motion Using Historical Aerial Images to Analyse Changes in Glacier Surface Elevation, Remote Sensing, 9, 1021, 2017, doi:10.3390/rs9101021

Naumann, M., Geist, M., Bill, R., Niemeyer, F. and Grenzdoerffer, G.: Accuracy comparison of digital surface models created by Unmanned Aerial Systems imagery and Terrestrial Laser Scanner, International Archives of the Photogrammetry, Remote Sensing and Spatial Information Sciences, UAV-g2013, 4-6 September 2013, Rostock, Germany, 61-W2, 281-286, 2013, doi: 10.5194/isprsarchives-XL-1-W2-281-2013

Nuth, C. and Kaab, A.: Co-registration and bias corrections of satellite elevation data sets for quantifying glacier thickness change, The Cryosphere, 5, 271-290, 2011, doi: 10.5194/tc-5-271-2011.

Oborne, M.: Mission planner software. Available at: http://ardupilot.org/planner/, last access: 18/05/2017, 2013.

O'Connor, J., Smith, M.J. and James, M.R.: Cameras and settings for aerial surveys in the geosciences: optimising image data, Progress in Physical Geography, 41, 1-20, 2017, doi: 10.1177/0309133317703092.

Palomo, I.: Climate Change Impacts on Ecosystem Services in High Mountain Areas: A Literature Review, Mountain Research and Development, 37,179-187, 2017, doi: 10.1659/MRD-JOURNAL-D-16-00110.1.

Piermattei, L., Carturan, L. and Guarnieri, A.: Use of terrestrial photogrammetry based on structure from motion for mass balance estimation of a small glacier in the Italian Alps. Earth Surface Processes and Landforms, 40, 1791-1802, 2015, doi: 10.1002/esp.3756.

Piermattei, L., Carturan, L., de Blasi, F., Tarolli, P., Dalla Fontana, G., Vettore, A. and Pfeifer, N.: Suitability of ground-based SfM–MVS for monitoring glacial and periglacial processes, Earth Surface Dynamics, 4, 325-443, 2016, doi: 10.5194/esurf-4-425-2016.

Pomerleau, F., Colas, F., Siegwart, R. and Magnenat, S.: Comparing ICP variants on real world data sets. Autonomous Robots, 34, 133–148, 2013, doi: 10.1007/s10514-013-9327-2.

Quincey, D.J., Lucas, R.M., Richardson. S.D., Glasser, N.F., Hambrey, N.J. and Reynolds, J.M.: Optical remote sensing techniques in high-mountain environments: application to glacial hazards, Progress in Physical Geography, 29, 475-505, 2005, doi: 10.1191/0309133305pp456ra.

Rayburg, S., Thoms, M. and Neave, M.: A comparison of digital elevation models generated from different data sources, Geomorphology, 106, 261-270, 2009, doi: 10.1016/j.geomorph.2008.11.007

Riccardi, A., Vassena, G., Scotti, R., Sgrenzaroli, M.: Recent evolution of the punta S.Matteo serac (Ortles-Cevedale Group, Italian Alps), Geografia Fisica e Dinamica Quaternaria, 33, 215-219, 2010.

Rolstad, C., Haug, T. and Denby, B.: Spatially integrated geodetic glacier mass balance and its uncertainty based on geostatistical analysis: application to the western Svartisen ice cap, Norway, Journal of Glaciology, 55, 666-680, 2009, doi: 10.3189/172756409787769528

Rounce, D.R., Watson, C.S. and McKinney, D.C.: Identification of Hazard and Risk for Glacial Lakes in the Nepal Himalaya Using Satellite Imagery from 2000–2015, Remote Sensing, 9, 654, 2017, doi:10.3390/rs9070654.

Ryan, J.C., Hubbard, A., Box, J.E., Brough, S., Cameron, K., Cook, J.M., Cooper, M., Doyle, S.H., Edwards, A., Holt, T., Irvine-Fynn, T., Jones, C., Pitcher, L.H., Rennermalm, A.K., Smith, L.C, Stibal, M. and Snooke, N.: Derivation of High Spatial Resolution Albedo from UAV Digital Imagery: Application over the Greenland Ice Sheet, Frontiers in Earth Science, 5, 40, 2017, doi: 10.3389/feart.2017.00040.

Seier, G., Kellerer-Pirklbauer, A., Wecht, M., Hirschmann, S., Kaufmann, V., Lieb, G.K. and Sulzer, W.: UAS-Based Change Detection of the Glacial and Proglacial Transition Zone at Pasterze Glacier, Austria. Remote Sensing, 9, 549, 2017, doi:10.3390/rs9060549.

Senese, A., Diolaiuti, G.A., Mihalcea, C. and Smiraglia, C.: Energy and Mass Balance of Forni Glacier (Stelvio National Park, Italian Alps) from a Four-Year Meteorological Data Record, Arctic, Antarctic and Alpine Research, 44, 122-134, 2012, doi: 10.1657/1938-4246-44.1.122.

Smiraglia, C., Azzoni, R.S., D'Agata, C., Maragno, D., Fugazza, D. and Diolaiuti, G.A.: The evolution of the Italian glaciers from the previous data base to the new Italian inventory. Preliminary considerations and results, Geogr. Fis. Dinam. Quat., 38, 79-87, 2015, doi: 10.4461/GFDQ.2015.38.08.

Teunissen, P.J.G.: Testing theory. An introduction. Series on Mathematical Geodesy and Positioning, VSSD Delft, The Netherlands, 2009.

Urbini, S., Zirizzotti, A., Baskaradas, J.A., Tabacco, I.E., Cafarella, L., Senese, A., Smiraglia, C., Diolaiuti, G.: Airborne radio echo sounding (RES) measures on alpine glaciers to evaluate ice thickness and bedrock geometry: Preliminary results from pilot tests performed in the ortles-cevedale group (Italian alps), Annals of Geophysics, 60, G0226, doi: 10.4401/ag-7122, 2017.

Vincent, C., Auclair, S. and Le Meur, E.: Outburst flood hazard for glacier-dammed Lac de Rochemelon, France, Journal of Glaciology, 56, 91-100, 2010, doi: 10.3189/002214310791190857

Vincent, C., Thibert, E., Harter, M., Soruco, A. and Gilbert, A.: Volume and frequency of ice avalanches from Taconnaz hanging glacier, French Alps, Annals of Glaciology, 56, 17-25, 2015, doi: 10.3189/2015AoG70A017.

Westoby, M.J., Brasington, J., Glasser, N.F., Hambrey, M.J. and Reynolds, J.M.: Structure-from-Motion' photogrammetry: A low-cost, effective tool for geoscience applications, Geomorphology, 179, 300-314, 2012, doi: 10.1016/j.geomorph.2012.08.021.

774 Winkler, M., Pfeffer, W.T. and Hanke, K.: Kilimanjaro ice cliff monitoring with close range
775 photogrammetry, International Archives of the Photogrammetry, Remote Sensing and Spatial
776 Information Sciences, XXII ISPRS Congress, Melbourne, Australia, 25 August-1 September 2012,
777 39-B5, 441-446, 2012.

778

Tables

DEM pair	Elevation differences without co-registration shifts ($\mu_{\Delta H} \pm \sigma_{\Delta H}$) [m]	Co-registration shifts		Elevation differences with co-registration shifts ($\mu_{\Delta H} \pm \sigma_{\Delta H}$) [m]
		X [m]	Y [m]	
2007-2014	1.96±2.60	1.11	-1.11	0.00±1.70
2007-2016	-0.43±3.48	2.44	-1.11	0.00±2.60
2014-2016	-2.92±3.21	-0.20	-1.30	0.00±2.22

Table 1: Statistics of the elevation differences between DEM pairs before and after the application of co-registration shifts. DEM 2007 from aerial multispectral survey, DEM 2014 and DEM 2016 from UAV photogrammetry.

Sample Window	Area (m^2)	Number of points in sample windows			Mean and standard deviation of point density [points/m^2]			Number of points above the lower 12.5% percentile		
		UAV	TP	TLS	UAV	TP.	TLS	UAV	TP	TLS
1	2793	-	1984k	141k	-	1654±637	226±100	-	880	26
2	1806	76k	2175k	130k	109±29	2297±708	391±217	61	881	0
3	495	43k	712k	25k	103±27	1978±606	151±60	49	766	31
4	672	62k	557k	33k	108±22	1384±530	141±69	62	324	2
5	3960	406k	810k	-	141±22	485±227	-	97	31	-

Table 2: Area and number of points in each sample window on the Forni Glacier terminus, mean and standard deviation of local point density and number of points above the lower 12.5% percentile in each window. k stands for thousands of points. UAV refers to UAV photogrammetry, TP to terrestrial photogrammetry and TLS to terrestrial laser scanning.

Sample Window		Means and Std. Dev.s of M3C2 distances [cm]			RMSE of M3C2 distances [cm]		
	Ref.	TLS	TLS	UAV	TLS	TLS	UAV
	Slave	TP	UAV	TP	TP	UAV	TP
1		4.5±7.4	-	-	8.7	-	-
2		-1.1±10.5	14.8±34.7	-14.5±26.7	10.6	37.7	30.4
3		8.4±4.1	14.7±15.1	-8.5±18.9	9.4	21.1	20.7
4		2.8±5.3	9.4±22.2	-2.3±24.9	6.0	24.0	25.0
5		-	-	-8.5±25.3	-	-	26.7

Table 3: Statistics on distances between point clouds computed on the basis of the M3C2 algorithm, showing mean, standard deviation and root mean square error (RMSE) of each point cloud pair. UAV refers to UAV photogrammetry, TP to terrestrial photogrammetry and TLS to terrestrial laser scanning. Ref. stands for reference and "-" means no comparison was performed.

DEM pair	Mean thickness change [m]	Mean thinning rates [ma^{-1}]	Volume Change [10^6 m^3]
2007-2014	-31.91 ± 1.70	-4.55 ± 0.24	-10.00 ± 0.17 (1.74%)
2007-2016	-42.86 ± 2.60	-4.76 ± 0.29	-13.46 ± 0.20 (1.47%)
2014-2016	-10.41 ± 2.22	-5.20 ± 1.11	-3.29 ± 0.08 (2.60%)

798 *Table 4: Average ice thickness change, thinning rates and volume loss from DEM differencing over*
799 *a common reference area of 0.32 km^2 for all DEM pairs. Uncertainty of thickness change expressed*
800 *as one standard deviation of residual elevation differences over stable areas after DEM co-*
801 *registration.*

802

Figures

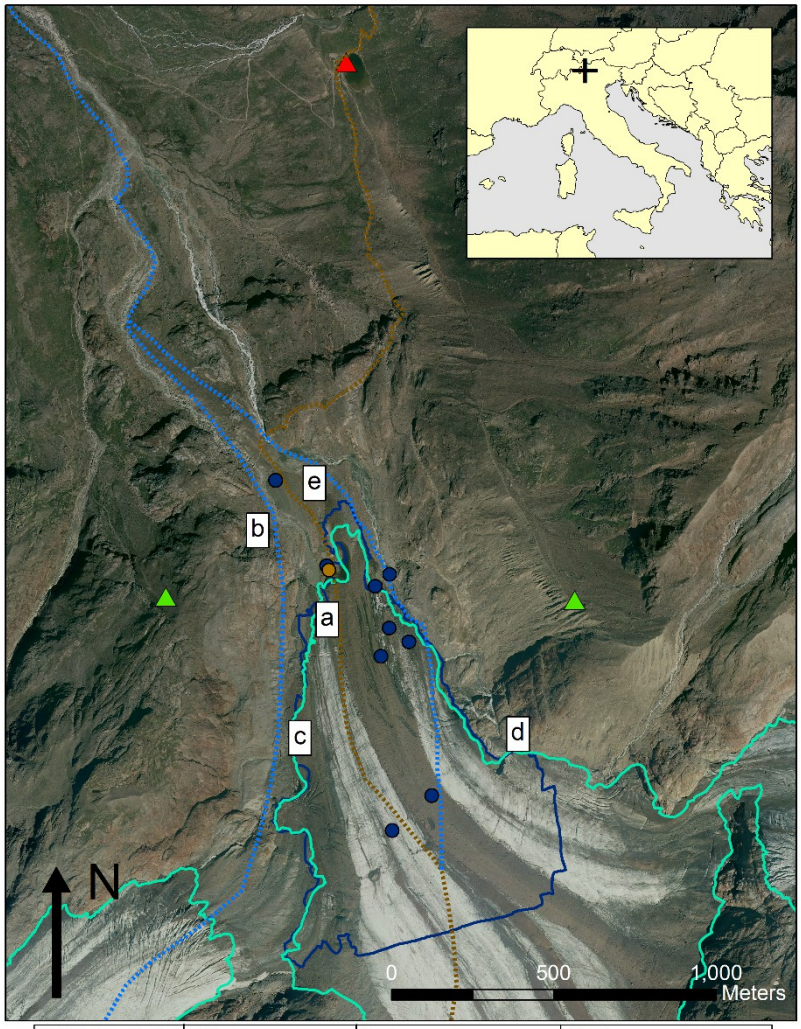

Figure 1: the tongue of Forni Glacier. The map shows the location of take-off/landing sites for the 2014 and 2016 UAV surveys, standpoint of TLS survey, GCPs used in the UAV photogrammetry surveys and trails crossing the glaciers. Letters a-e identify the location of features described in Fig.2. Base map from 2015 courtesy of IIT Regione Lombardia WMS Service. Trails from Kompass online cartography at https://www.kompass-italia.it/info/mappa-online/..

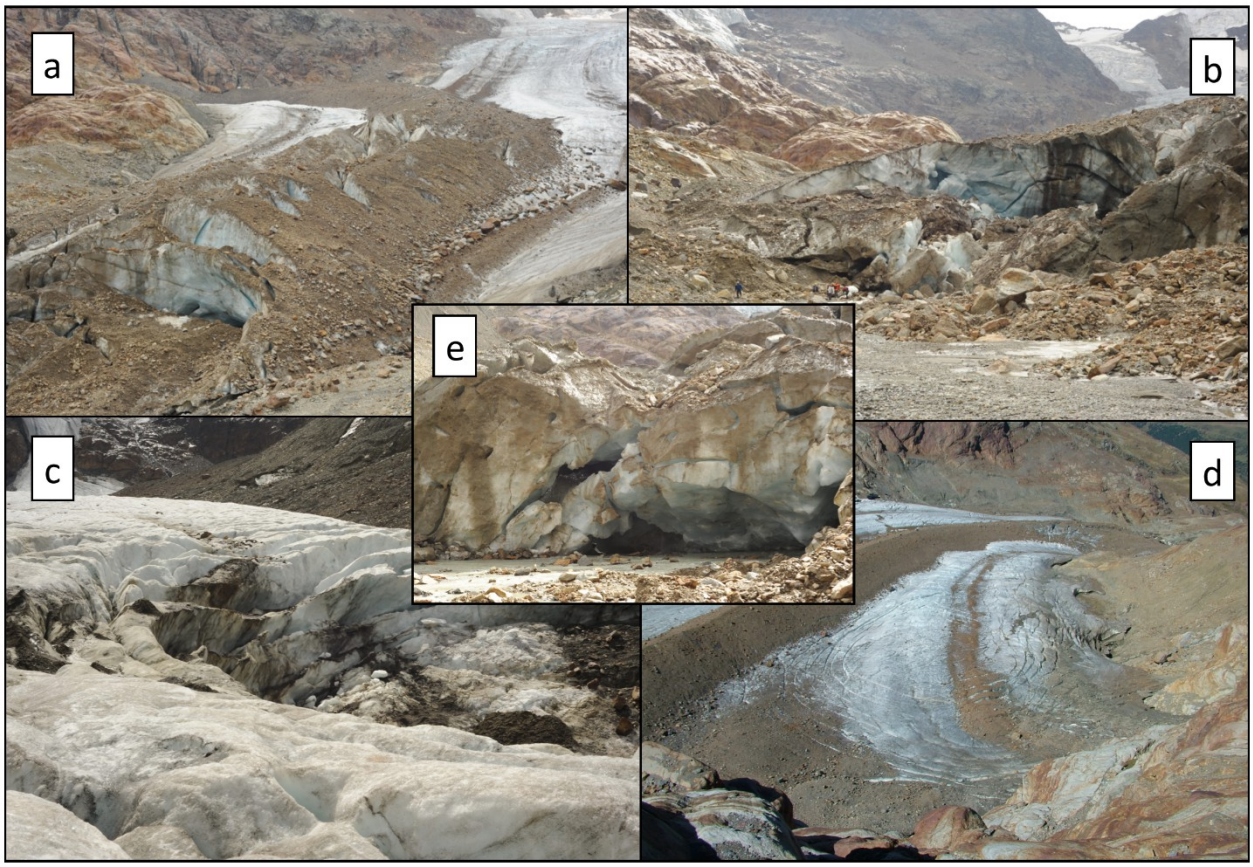

Figure 2: Collapsing areas on the tongue of Forni Glacier. (a) Faults cutting across the eastern medial moraine; (b) glacier terminus; (c) Near-circular collapsed area on the central tongue; (d) Large ring fault on the eastern tongue at the base of the icefall. Photo courtesy of G.Cola; (e) Close-up of a vertical ice cliff at the glacier terminus. The location of features is reported in Fig.1

Aircraft type	Swinglet CAM, Commercial platform
Digital Camera	Canon Ixus 127 HS
Camera technical features	16 Megapixel, focal length 4.3 mm
GNSS antenna	GPS only
Weight (incl. payload)	0.50 Kg
Battery time	30 minutes

Aircraft type	Customized, with Tarot frame 650 size, VR Brain 5.2 Autopilot & APM Arducopter 3.2.1 Firmware
Digital camera	Canon Powershot ELPH 320 HS
Camera technical features	16 Megapixel, focal length 4.3 mm
GNSS antenna	GPS+GLONASS (Galileo compatible)
Weight (incl. pay-load)	2.75 Kg
Battery time	20-25 minutes

820

821 *Figure 3: The UAVs used in surveys of the Forni Glacier and their characteristics. (a) The*
822 *SwingletCam fixed-wing aircraft employed in 2014, at its take off site by Lake Rosole; (b) The*
823 *customized quadcopter used in 2016 in the lab.*

824

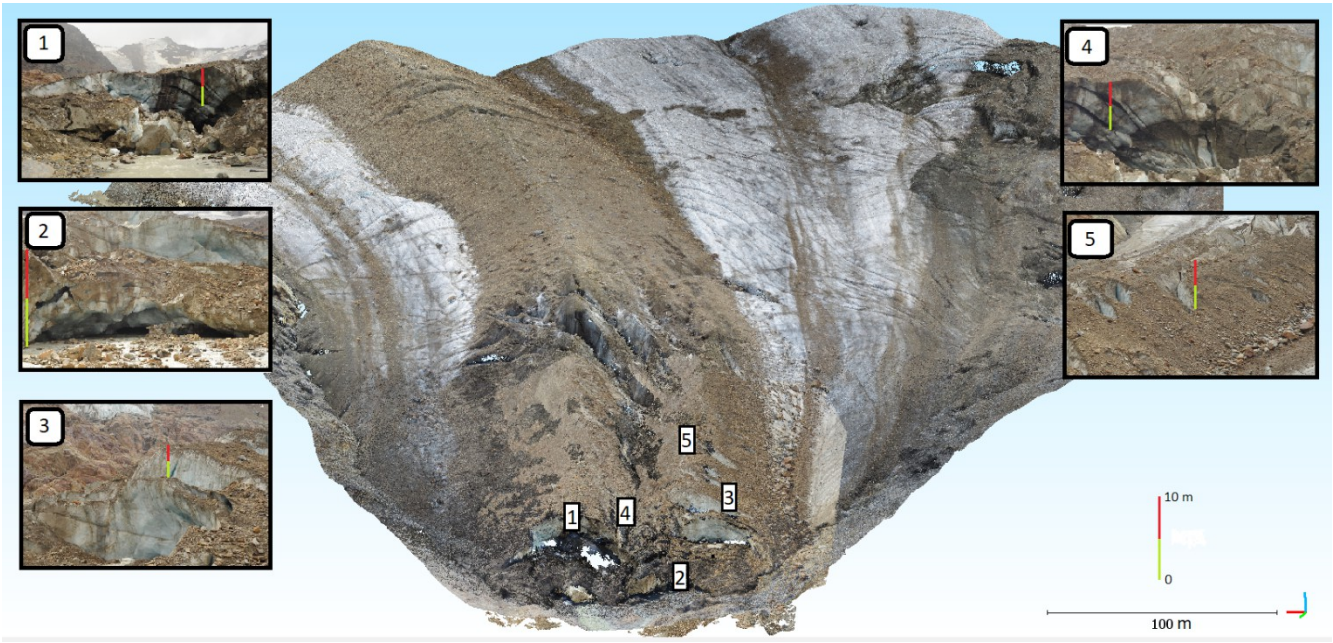

Figure 4: Location of different glacier features or hazard-prone areas on the tongue of Forni glacier were the point cloud comparison was performed. The background image is the merged point cloud generated from the 2016 UAV and terrestrial photogrammetry survey.

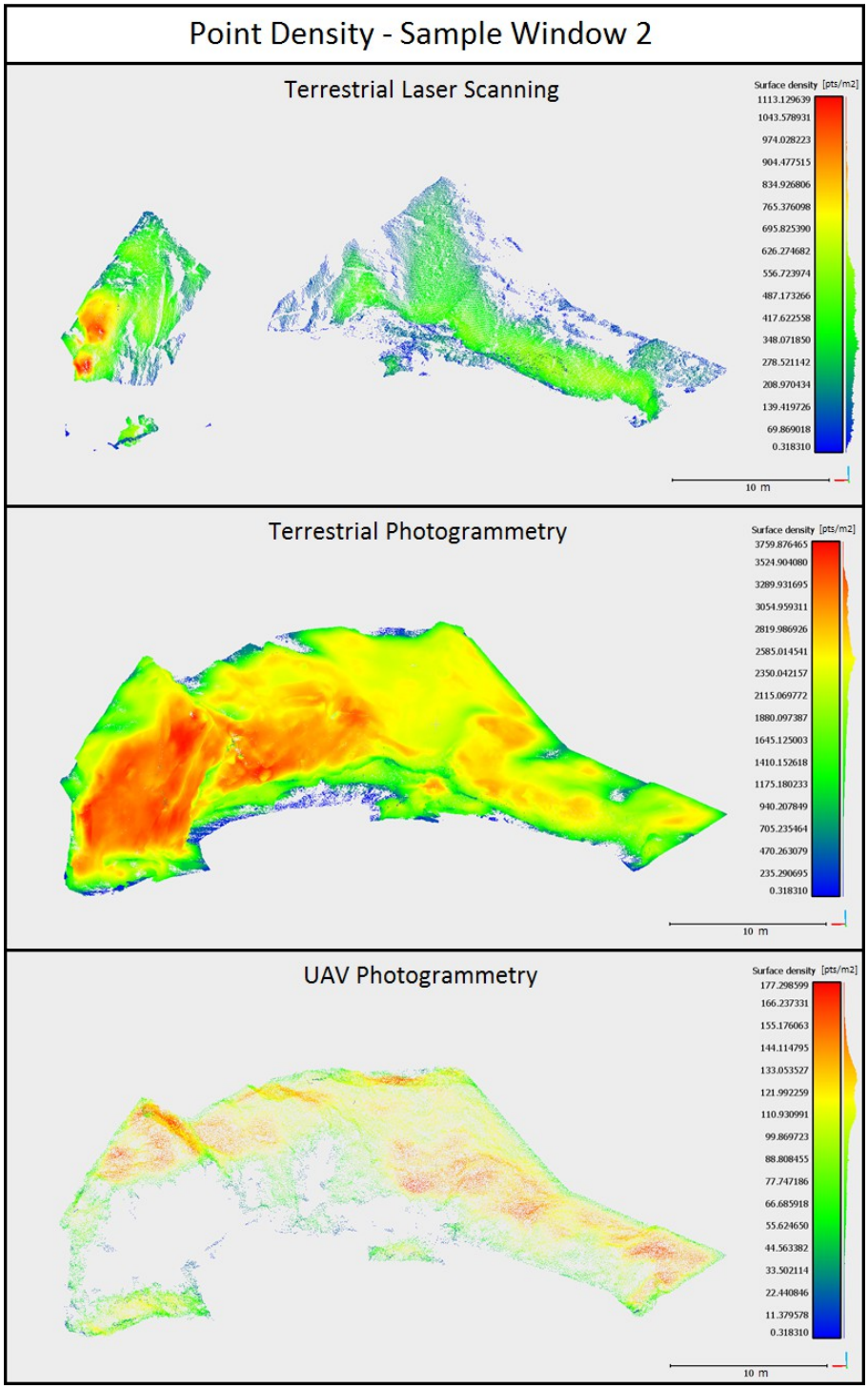

830

831 *Figure 5: Maps of point density in sample location 2.*

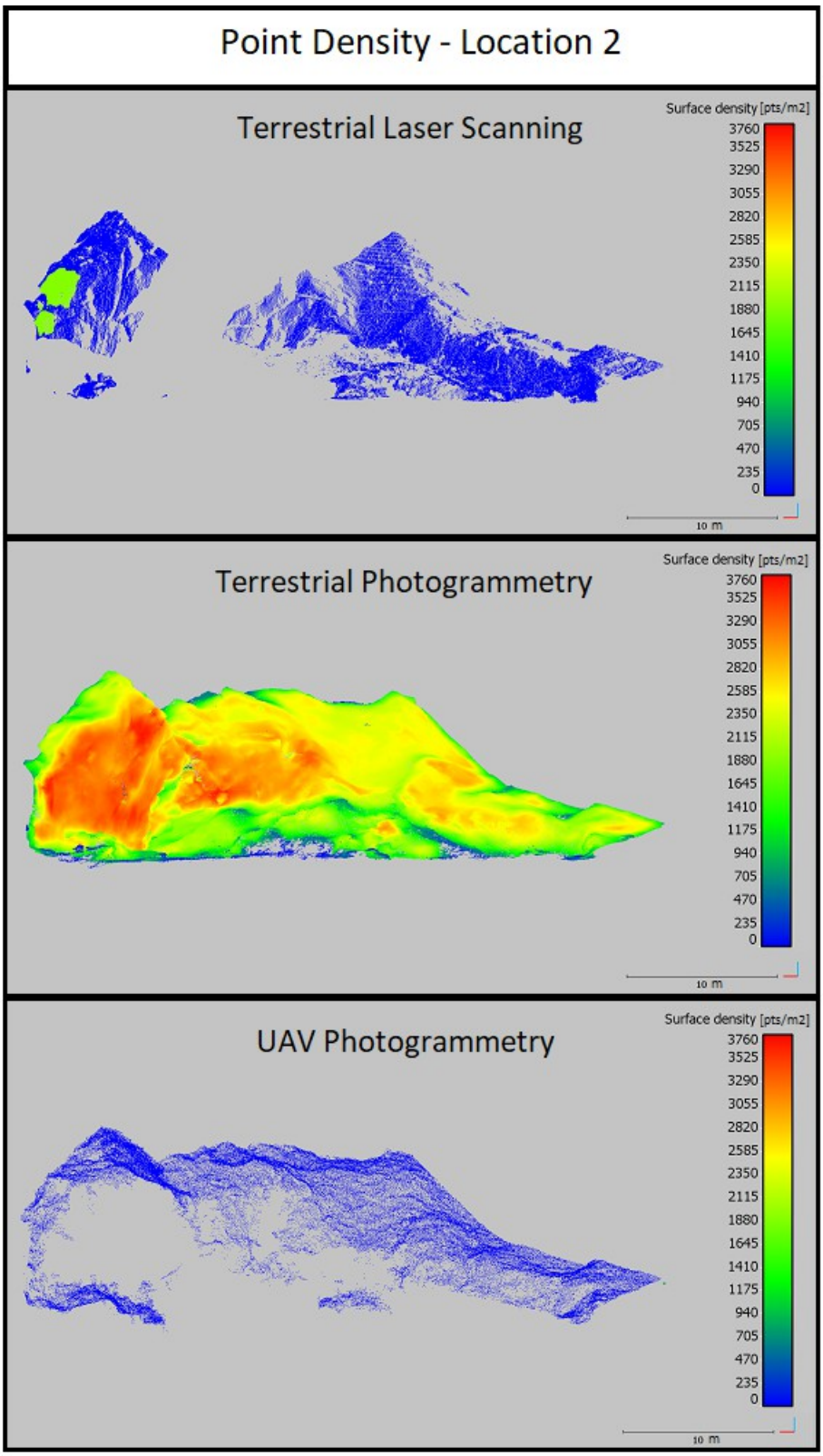

832

833 *Figure 5 (alternative): Maps of point density in sample location 2.*

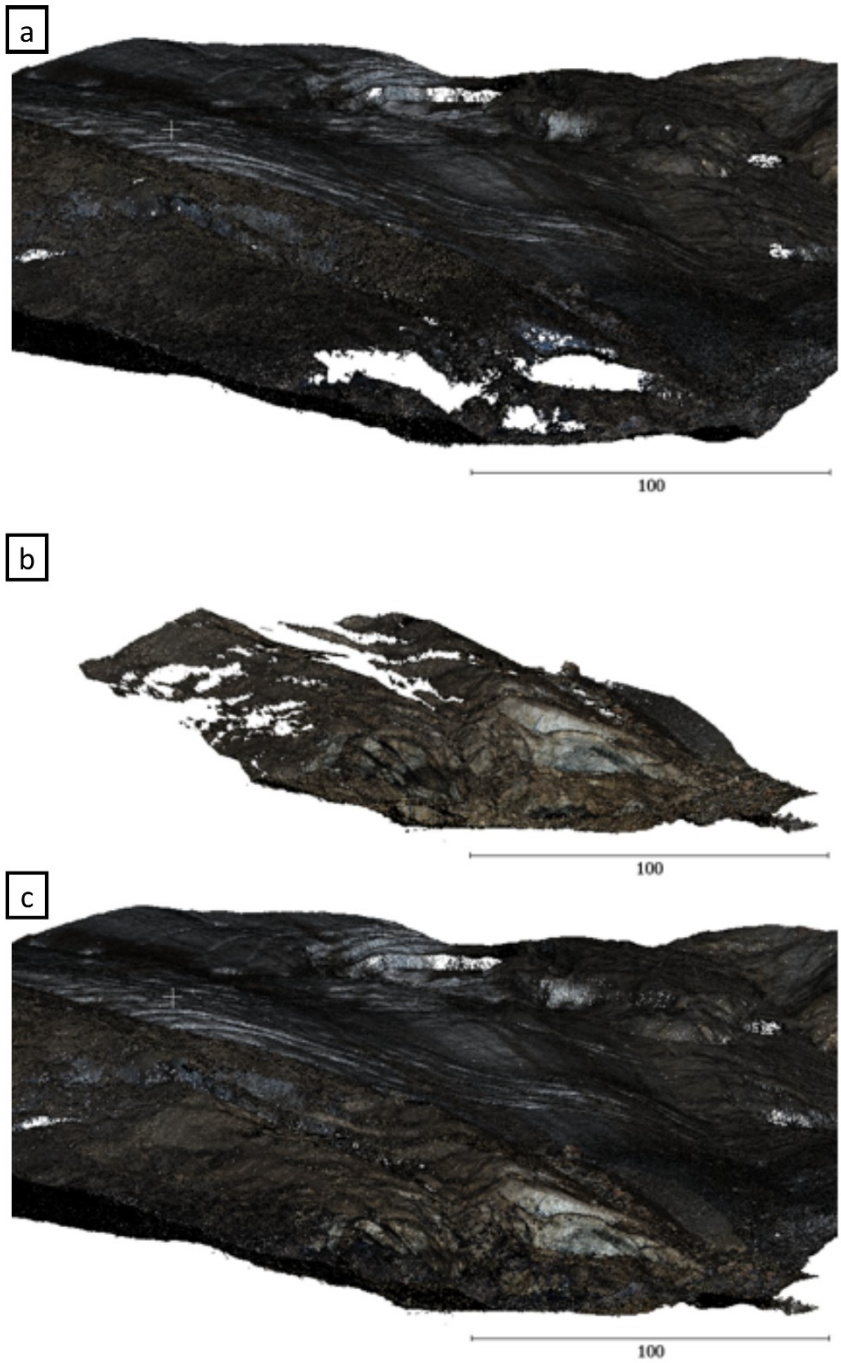

834

835 *Figure 6: Spatial coverage of UAV- and terrestrial photogrammetry point clouds and merged point*
836 *cloud from the two techniques. a) UAV photogrammetry point cloud; b) terrestrial photogrammetry*
837 *point cloud; c) merged point cloud.*

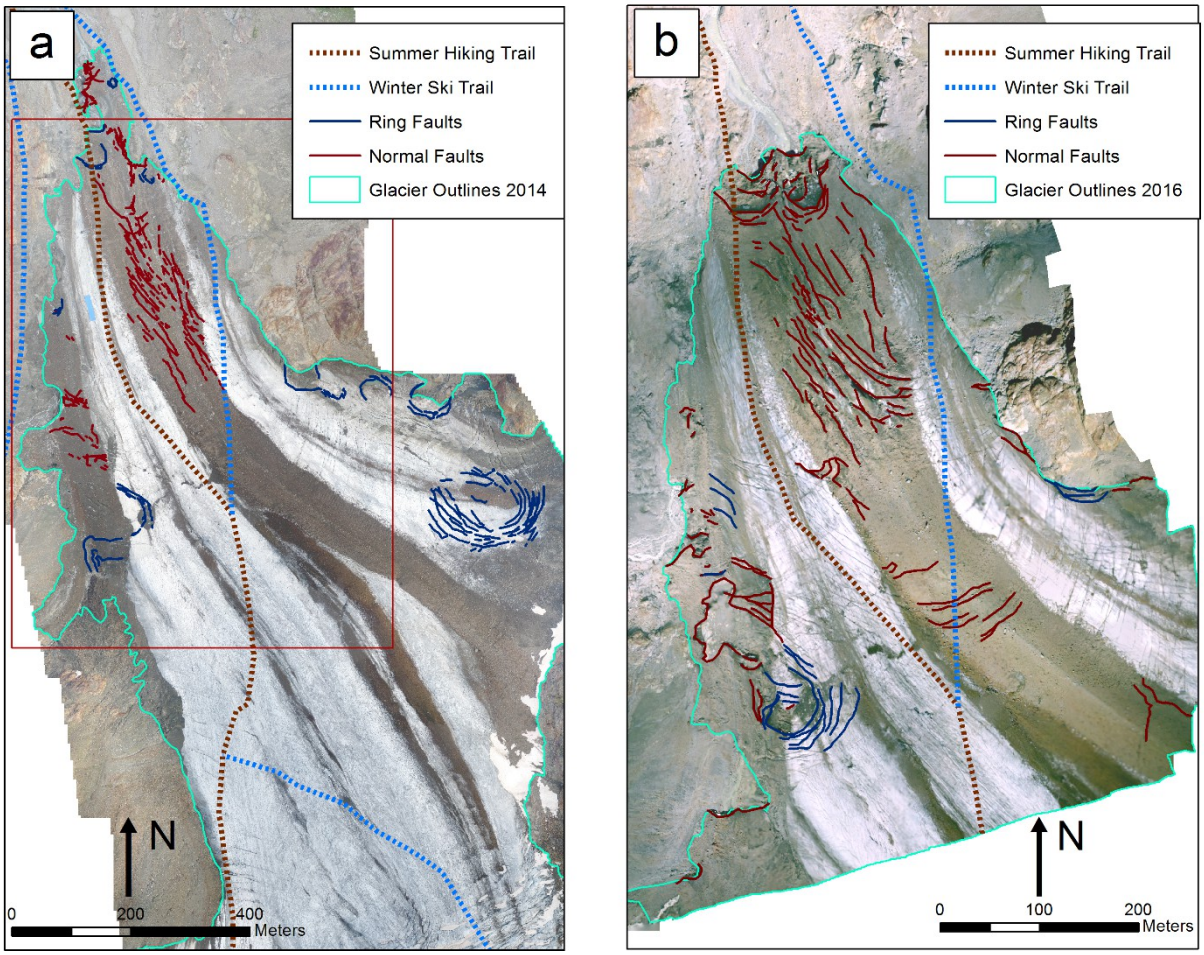
a
Summer Hiking Trail
Winter Ski Trail
Ring Faults
Normal Faults
Glacier Outlines 2014
N
0
200
400
Meters
b
Summer Hiking Trail
Winter Ski Trail
Ring Faults
Normal Faults
Glacier Outlines 2016
N
0
100
200
Meters

838

839 *Figure 7: Location of collapse structures, i.e. normal faults and ring faults and trails crossing the*
840 *Forni Glacier. (a) Collapse structures in 2014, with 2014 UAV ortophoto as basemap. The red box*
841 *marks the area surveyed in 2016. (b) Collapse structures in 2016, with 2016 UAV orthophoto as*
842 *basemap. Trails from Kompass online cartography at https://www.kompass-*1039 *italia.it/info/map-*
843 *pa-online/.*

844

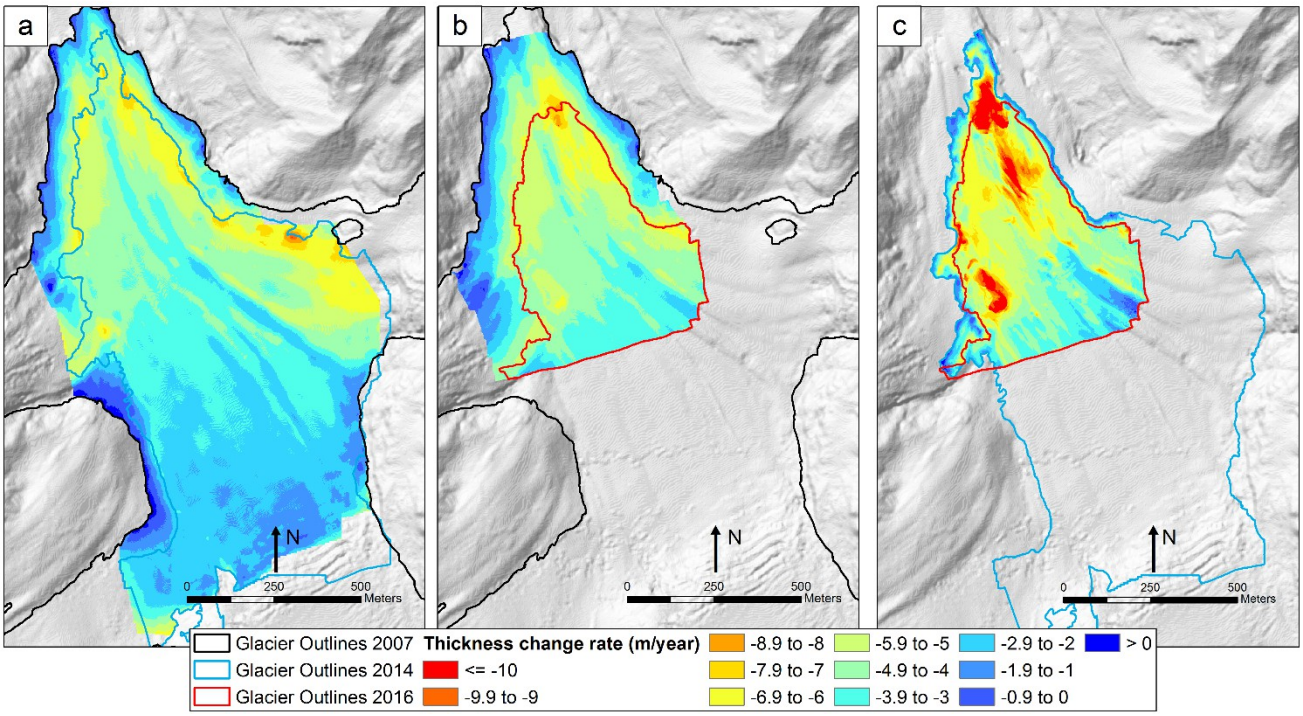

Figure 8: Ice thickness change rates from DEM differencing over (a) 2007-2014; (b) 2007-2016; (c) 2014-2016. Glacier outlines from 2014 and 2016 are limited to the area surveyed during the UAV campaigns. Base map from hillshading of 2007 DEM.